





## Stratigraphic and structural control over permeability distribution in poorly consolidated siliciclastic rocks

*Controle estratigráfico e estrutural sobre a distribuição da permeabilidade em rochas siliciclásticas pouco consolidadas*

Thayssa Pereira de Andrade<sup>1</sup> , Emilio Velloso Barroso<sup>1</sup> , Luis Paulo Vieira Braga<sup>1</sup> ,  
Claudio Limeira Mello<sup>1</sup> , Jorge André Braz de Souza<sup>2</sup> 

<sup>1</sup>Universidade Federal do Rio de Janeiro - UFRJ, Instituto de Geociências, Departamento de Geologia, Centro de Ciências Matemáticas e da Natureza, Programa de Pós-graduação em Geologia, Avenida Athos da Silveira, 274, Ilha do Fundão, Cidade Universitária, CEP: 21949-900, Rio de Janeiro, RJ, BR (andrade@geologia.ufrj.br; emilio@geologia.ufrj.br; lpbraga@geologia.ufrj.br; limeira@geologia.ufrj.br)

<sup>2</sup>Centro de Pesquisas Leopoldo Américo Miguez de Mello - CENPES-Petrobras, Rio de Janeiro, RJ, BR (jorgeabs@petrobras.com.br)

Received on August 11, 2020; accepted on April 23, 2021.

### Abstract

Permeability models are very relevant for the characterization of oil systems. However, limitations related to the resolution of seismic data make it difficult to identify subseismic, sedimentary, and tectonic structures, which can significantly impact the flow pattern. This study analyzed the spatial variability of permeability according to stratigraphic and structural geology control to propose a useful model for poorly consolidated, fractured, and faulted siliciclastic reservoirs. In an outcrop analogue to this type of reservoir, air permeability was measured in 3 orthogonal directions at 24 points, spaced 2 m apart. The models were obtained by sequential Gaussian simulation (SGS) after statistical data treatment. The models were validated to ensure the consistency of the generated scenarios. Permeability values showed a positive asymmetric distribution and reduced medians toward tectonic structures. The fitted semivariogram model was exponential, with higher spatial continuity in the horizontal flow direction and lower in the vertical one. The permeability models emphasized the importance of considering subseismic structures in the flow analysis of reservoirs since they have proven to play a significant role in the permeability distribution in the outcrop assessed.

**Keywords:** Permeability; Geostatistical simulation; Litho-structural control.

### Resumo

Modelos de permeabilidade têm grande relevância na caracterização de sistemas petrolíferos. Contudo, limitações relacionadas à resolução dos dados sísmicos adquiridos tornam difícil a identificação de estruturas subsísmicas, sedimentares e tectônicas, que podem ter grande impacto no padrão de fluxo. Neste trabalho, foi analisada a variabilidade espacial da permeabilidade segundo o controle da estratigrafia e da geologia estrutural, tendo como finalidade propor um modelo que possa ser empregado em reservatórios siliciclásticos pouco consolidados, fraturados e falhados. Em um afloramento análogo a esse tipo de reservatório foram realizadas leituras de permeabilidade ao ar em três direções ortogonais de 24 pontos espaçados de 2 m. Os modelos foram obtidos a partir da simulação sequencial gaussiana (SSG), após o tratamento estatístico dos dados. A validação dos modelos foi realizada para assegurar a consistência dos cenários gerados. As permeabilidades apresentaram distribuição assimétrica positiva e diminuição das medianas em direção às estruturas tectônicas. O modelo de ajuste dos semivariogramas foi o exponencial, sendo a continuidade espacial maior na direção de fluxo horizontal e menor na direção de fluxo vertical. Os modelos de permeabilidade ressaltaram a importância de considerar estruturas subsísmicas na análise de fluxo em reservatórios, uma vez que essas mostraram desempenhar papel relevante na distribuição da permeabilidade no afloramento análogo analisado.

**Palavras-chave:** Permeabilidade; Simulação geoestatística; Controle litoestrutural.

## INTRODUCTION

Understanding the spatial distribution of permeability is very relevant for the characterization of oil systems, as well as for evaluating the feasibility of exploiting reservoirs and determining the strategy for the development and management of field production. Data acquisition for the analysis of this distribution in reservoirs has some limitations, either due to the restricted number of samples that can be tested by observation or to the low resolution of seismic data, making it difficult to identify subseismic structures that can influence flow patterns (Slatt, 2006).

Different authors address the use of outcrop analogues as a tool to characterize real reservoirs (Souza, 2013; Pyrcz and Deutsch, 2014; Maciel et al., 2017; Belila et al., 2018; Galvão et al., 2018). They argue that this procedure enables more detailed analyses of the influence of lithological variations, sedimentary facies, and smaller tectonic structures on the mechanical and hydraulic properties of rocks. Geostatistics has been widely used to predict permeability values, considering both rocks and structures (e.g., faults), and thus construct models that characterize different reservoirs (Pyrcz and Deutsch, 2014). Many techniques have been applied in the development of permeability models, including ordinary kriging (Wilson et al., 2011), kriging with external drift (Camargo and Jensen, 2012), co-simulation using permeability and porosity (Fegh et al., 2012; Cao et al., 2014), simple cokriging, ordinary cokriging (Zhao et al., 2014), and sequential Gaussian simulation — SGS (Hosseini et al., 2019; Ren et al., 2019). The results generated by these models have been improved by geostatistical methods, bypassing the issue of discontinuous sampling. Among these methods, geostatistical simulations are often used due to their capacity to better characterize heterogeneity in higher-detail scales (Ren et al., 2019) and quantify uncertainty by producing different scenarios (Hosseini et al., 2019).

This article aimed to analyze the influence of lithological and structural framework on the spatial distribution of permeability to propose a permeability model for poorly consolidated and fractured siliciclastic reservoirs.

## REGIONAL GEOLOGICAL CONTEXT AND THE OUTCROP ANALOGUE

The Volta Redonda Basin is located in the central segment of the Continental Rift of Southeastern Brazil (*Rift Continental do Sudeste do Brasil* — RCSB), in the Ribeira Belt domain, and is predominantly seated on metasedimentary successions of the Paraíba do Sul Complex (Riccomini et al., 2004; Sanson et al., 2006). The Casa de Pedra Graben is an elongated tectonic depression in the ENE-WSW direction

covering 13 km<sup>2</sup> and has the best-preserved Cenozoic sedimentary deposits of the Volta Redonda Basin (Riccomini et al., 2004; Sanson et al., 2006).

The Resende Formation, of Eocene age, corresponds to the main sedimentary stage of the basin and is characterized by the alternation of grano-decreasing cycles of stratified feldspar sandstone and thin layers of fine conglomerates, with possible layers of solid greenish mudstone and poorly selected rudites (Sanson et al., 2006; Negrão et al., 2015). Incomplete sedimentary cycles marked by erosive contacts are common at the base of conglomerate and sandstone layers (Maciel et al., 2017).

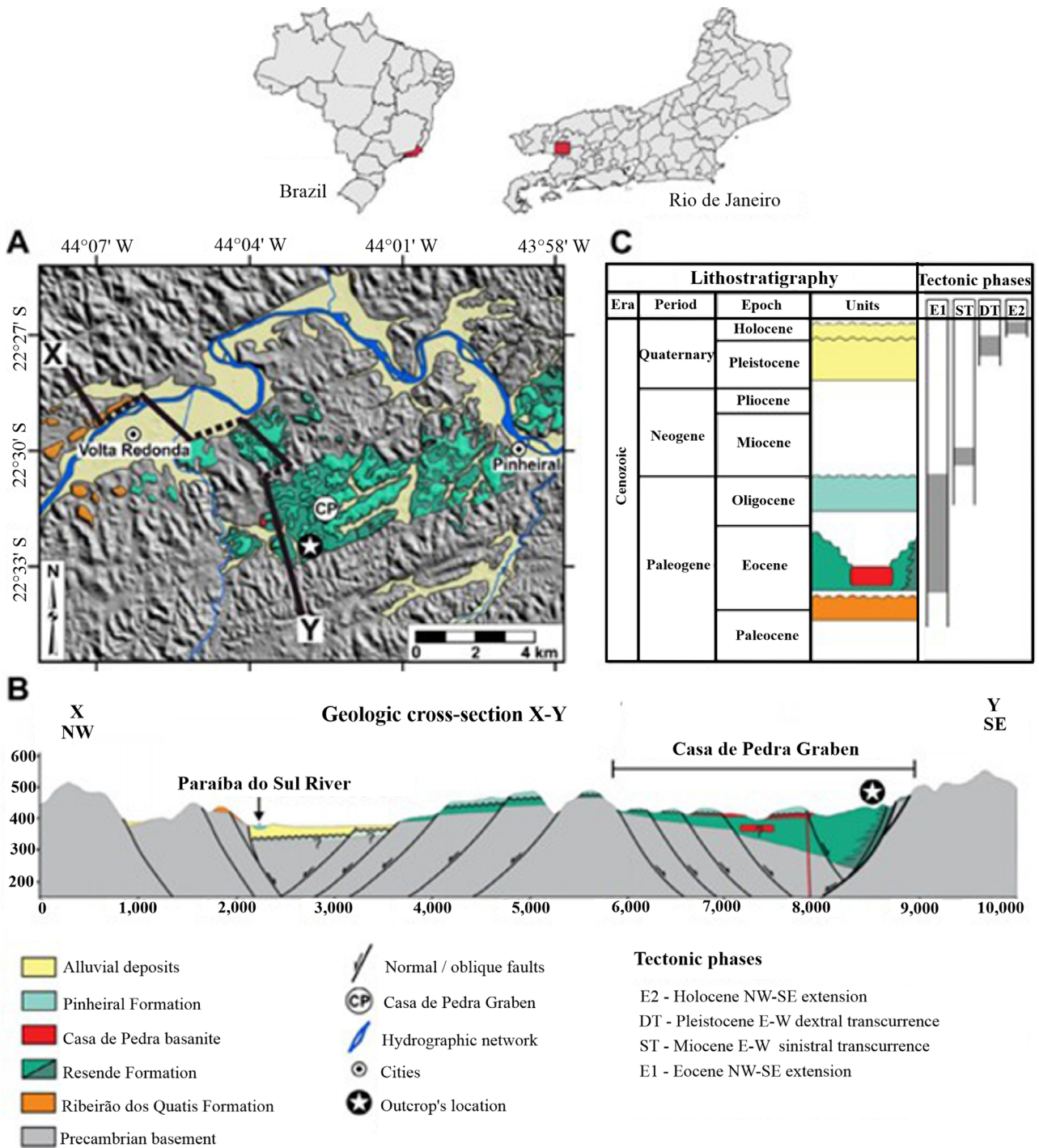
The movement of the main basin fault allowed the development of small alluvial fans and a river system with predominantly SE paleoflow. This unit is interpreted as associated with alluvial fans interfingering with axial fluvial systems with braided patterns (Sanson et al., 2006).

The outcrop selected for this study, regarded as geomaterial analogue to poorly consolidated and fractured siliciclastic reservoirs (Maciel et al., 2017), is located near the southern edge of the Casa de Pedra Graben, in a private field close to the Contorno Highway, in Rio de Janeiro (Figure 1). It is divided into three blocks separated by two main normal faults, F1 and F2, of ENE-WSW orientation and opposite dips (Maciel et al., 2017) (Figure 2A). This paper analyzed the horst in relation to the F1 fault (H-F1). This horst is located in the southern part of the outcrop (Figure 2B), whose approximate dimension is 18 m wide and 10 m high. This block was selected for its variety in structural features (deformation band clusters and fault) and layers with sedimentary characteristics (granulometry, texture, and facies), making it of interest when evaluating whether the geostatistical simulation is capable of capturing the diverse geological features that affect the outcrop permeability model.

## METHOD

The characterization steps were based on field, laboratory, and exploratory data analysis procedures.

The characterization of the spatial distribution of air permeability was performed *in situ* with the mini-permeameter TinyPerm3, handheld equipment manufactured by the New England Research (NER). When the mobile piston filled with air is pressed against the sample surface, the equipment monitors the transient flow and the air volume variation, providing the air permeability value of the tested medium. The manufacturer of TinyPerm3 recommends taking permeability measurements at the factory calibration interval — 1 mD to 10 D (Brown and Smith, 2013). Balsamo et al. (2013), working with highly permeable sediments from the Barreiras Formation, detected values greater than 10 D, as was the case in this work (“Results” section). These authors



Source: Negrão et al. (2015); modified by Fiuza et al. (2020).

**Figure 1.** (A) Geological map of the Volta Redonda Basin region; (B) schematic geological section, whose location is presented in (A); (C) lithostratigraphic column and tectonic phases identified in the Volta Redonda Basin.

reported a new calibration performed by the manufacturer, demonstrating that the calibration equation is preserved for values up to 5,000 D, although individual measurements are slightly more uncertain. The maximum air permeability values

in this study are around 100 D, guaranteeing the precision and accuracy of the data presented in this paper.

Before measuring the permeability, the surfaces were prepared to minimize the influence of superficial weathering,



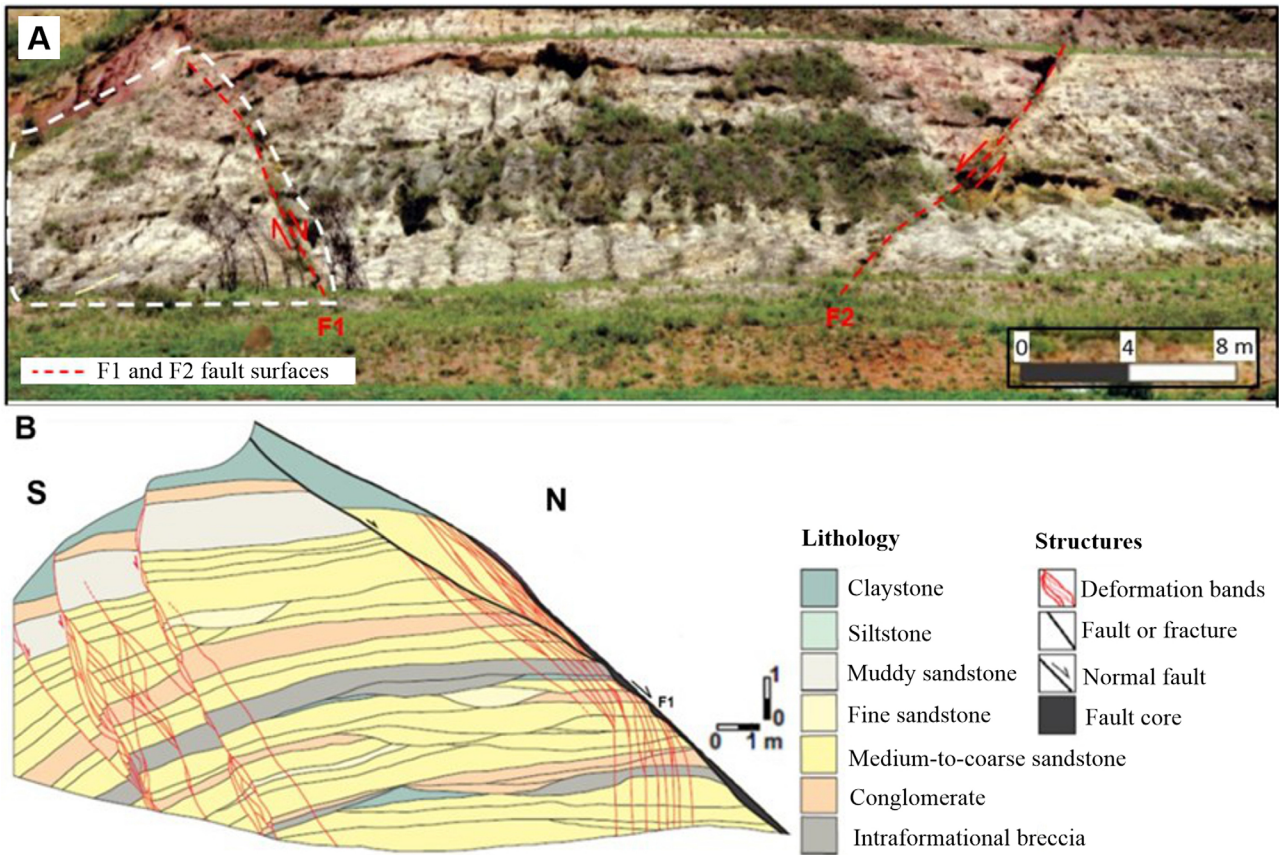


**Figure 2.** (A) Image of the outcrop (Maciel et al., 2017) and (B) geological section at a 1:50 scale, produced by Fiuza (2019). The white polygon in (B) highlights the block analyzed in the present study.

avoid air escape during the test (Souza, 2013), and have all measurements in the same coordinate axis (Figure 3). Thus, with the aid of a compass and a scraper, three orthogonal flat surfaces were prepared at each test point.

The acquisition of permeability data and the sample removal followed two types of deterministic sampling: total and restricted. According to Cressie (1991), systematic sampling assumes that the first position is randomly chosen; when this does not occur, sampling is called deterministic or regular non-random. The total deterministic sampling integrated permeability readings in the center of each grid cell of the outcrop section (Fiuza, 2019; Fiuza et al., 2020). For all points, approximately ten permeability measurements were taken in each of the three orthogonal flow directions assessed: horizontal perpendicular to the fault, horizontal parallel to the fault, and vertical.

The restricted deterministic sampling consisted of obtaining fault permeability readings with repetitions of five measurements per point. The irregularity and difficult preparation of the fault surface — due to its low thickness and rigidity caused by oxidation by iron oxide (Figure 4) — made

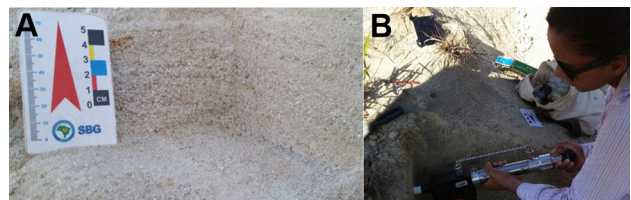


**Figure 3.** (A) Surfaces prepared for measurements and (B) air permeameter TinyPerm3.



**Figure 4.** Fault surface.



it challenging to read its permeability. Therefore, the measurements were obtained perpendicular to the fault plane, and the rock in the fault plane was interpreted as isotropic regarding permeability. These measurements were considered control points and used to ensure the representativeness of the faults in the produced simulations.

The granulometric characterization of sampling points followed the ABNT regulation, NBR 7181/2016 (*Solo – Análise Granulométrica*) (ABNT, 2016), and the results were categorized according to Folk's (1974) ternary diagram, based on Wentworth's (1922) grain size classification.

The statistical analysis comprised the steps:

- data treatment, which excluded field permeability readings obtained in tests with execution errors and outliers (defined as values 1.5 times the interquartile range added to the third quartile or subtracted from the first quartile) for each set of points per direction;
- descriptive statistics ( $\bar{M}$ : mean;  $Q_2$ : median;  $\sigma$ : standard deviation; IQR: interquartile range; min: minimum; max: maximum; CV: coefficient of variation), which analyzed data distribution and defined the characteristic permeability ( $\bar{k}$ ) of each direction as the most representative statistics according to data distribution (characteristic permeability of horizontal flow perpendicular to the fault —  $\bar{k}_{\text{perp}}$ , characteristic permeability of horizontal flow parallel to the fault —  $\bar{k}_{\text{para}}$ , and characteristic permeability of vertical flow —  $\bar{k}_{\text{vert}}$ ).

Due to the asymmetric data distribution, both in the analysis of all values obtained (as seen in the “Results” section) and of the repeated permeability readings in each sample, the median set of values was defined as the  $\bar{k}$  of each direction per point.

The geostatistical phase involved spatial data analysis (bubble plot and variography), SGS, and validation, based on  $\bar{k}$  data. The semivariogram measures the difference between pairs of points separated by distance  $h$  (Equation 1):

$$\gamma(h) = \frac{1}{2N(h)} \sum_{\alpha=1}^{N(h)} [z(u_{\alpha}) - z(u_{\alpha} + h)]^2 \quad (1)$$

In which:

$N(h)$  = number of pairs separated by distance  $h$ ;

$z(u_{\alpha})$  and  $z(u_{\alpha} + h)$  = measured values;

$u_{\alpha}$  and  $u_{\alpha} + h$  = coordinates in the plane or space separated from each other by distance  $h$ .

Among different simulation methods, SGS is often adopted for reservoir modeling. It is a simple, flexible, reasonably efficient method (Pyrzcz and Deutsch, 2014), capable of showing better heterogeneity characterization in higher precision scales (Ren et al., 2019). Simulation is part of a set of probabilistic models, which are based on data and provide numerous possible results.

Validating the simulations generated is an important geostatistical analysis step, as it attests to the consistency of the model. This step can be performed through different methods, such as cross-validation and jackknife (Leuangthong et al., 2004; Braga, 2014; Pyrcz and Deutsch, 2014; Hosseini et al., 2019). The present study employed the method defined by Leuangthong et al. (2004) as minimum criteria. This method is based on the assumption that the simulation should reproduce the characteristics of experimental data. To this end, its criteria are:

1. Simulated values at the sampling points must coincide with experimental data;
2. The histogram of simulated values should be similar to that of experimental data;
3. The same should be true for basic statistics;
4. The semivariogram (or covariogram) of simulated values should be similar to that of the observed values (Leuangthong et al., 2004; Braga, 2014).

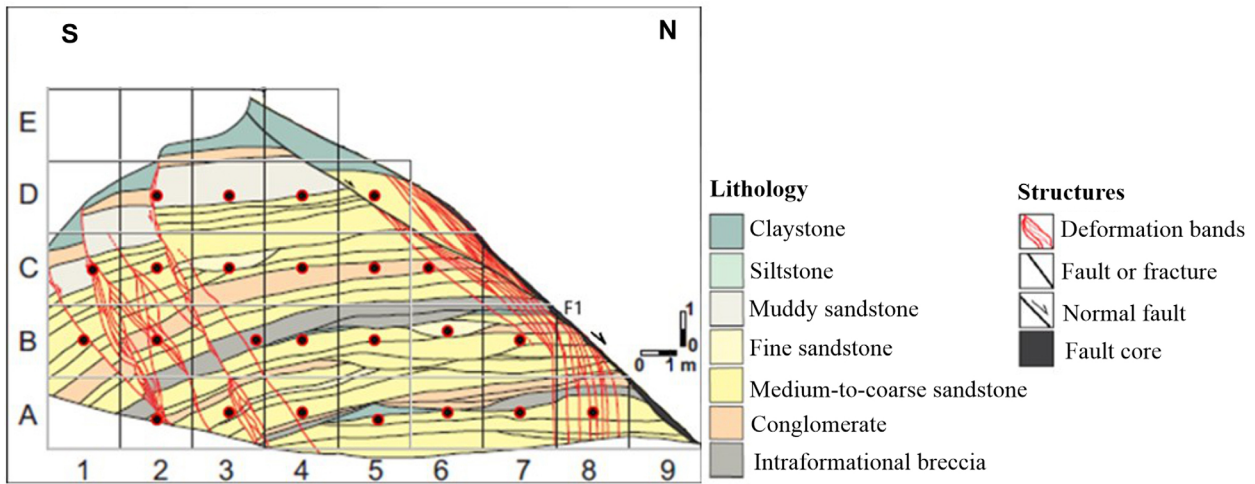
The present study presents only criteria 2, 3, and 4 since criterion 1 is ensured by the exact interpolation kriging property. The geostatistical stage was developed using the Gstat package (Pebesma and Wesseling, 1998) of the R software (R Core Team, 2018).

## RESULTS AND DISCUSSION

Deterministic sampling resulted in the analysis of 24 points (Figure 5) and a total of 849 permeability readings, among which 52 were outliers. Based on the units defined by Fiuza (2019) when mapping the geological section, medium-to-coarse sandstone (62.5%) is the main rock in the sampling points, followed by conglomerate (23%). Regarding Folk's (1974) rock textural classification, the predominant classes are muddy sandstone — MS (37.5%) and slightly gravelly muddy sandstone — SGMS (37.5%), as presented in Table 1. We emphasize that the percentages reported herein refer to the number of total points in each rock in relation to the number of points sampled.

Considering all readings taken (Figure 6) — including outliers —, the 3 directions showed unimodal distribution with positive asymmetry, values ranging from  $6 \times 10^{-4} D$  (total minimum value, obtained in  $\bar{k}_{\text{para}}$ ) to  $130 D$  (total maximum value, obtained in  $\bar{k}_{\text{vert}}$ ), and medians concentrated in intervals up to  $10 D$ . The dispersion of values reflects the lithology, the textural variations in the units, and the proximity to the structures (deformation bands and faults).

The  $\bar{k}$  box plot of all cells (Figure 7) demonstrated similar distribution and basic statistics, with the horizontal parallel and vertical directions presenting, respectively, greater and lower dispersion of  $\bar{k}$  values when considering the interquartile range.



Source: modified from Fiuzza (2019).

**Figure 5.** Distribution of sampling points according to the geological section of the outcrop.

**Table 1.** Lithology of the sampled points according to field description (Fiuzza, 2019) and granulometric analysis. The frequency refers to the total sampled points for each rock.

Geological section of the outcrop			Folk's ternary diagram		
Rock	Freq.	%	Rock	Freq.	%
Medium-to-coarse sandstone	15	62.5	Muddy sandstone	9	37.5
Conglomerate	4	16.7	Slightly gravelly muddy sandstone	9	37.5
Fine sandstone	2	8.3	Gravelly muddy sandstone	6	25
Muddy sandstone	2	8.3			
Intraformational breccia	1	4.2			

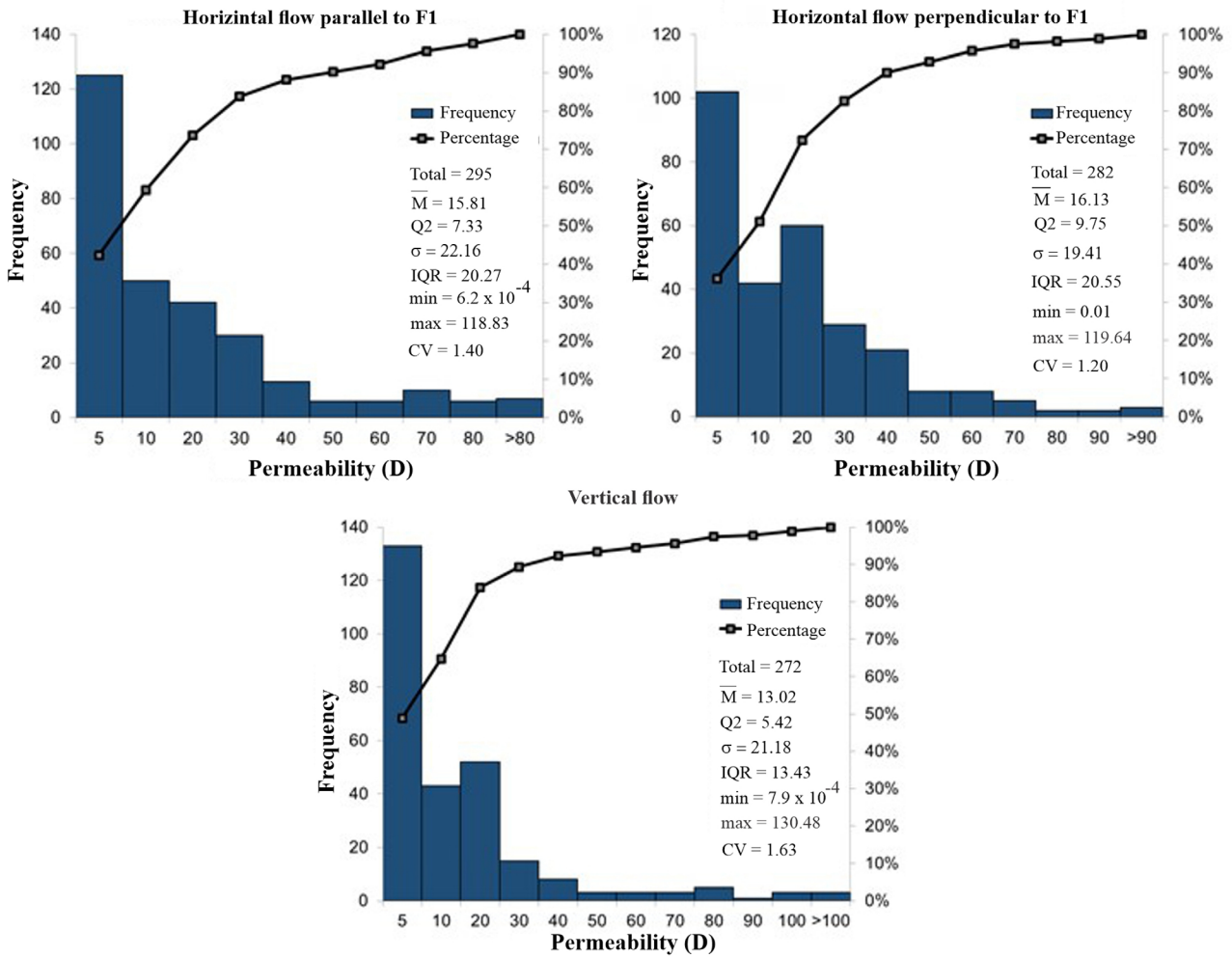
The ternary diagram of relative proportion between permeability values (Figure 8A) shows the degree of anisotropy per sample, defined by the proportional permeability value among the three directions, that is, isotropic samples are located in the center of the diagram, while those near the vertices indicate a high degree of anisotropy (Farrell et al., 2014). As the similarity of data distribution suggests, a low degree of anisotropy is common, with few points of higher expression. The median, mean, and maximum ratio corresponded, respectively, to 1.3, 3.6, and 20.4 for  $\bar{k}_{\text{perp}}/\bar{k}_{\text{vert}}$ , and to 1.1, 2.8, and 27.9 for  $\bar{k}_{\text{para}}/\bar{k}_{\text{vert}}$ . Among horizontal permeability values —  $\bar{k}_{\text{para}}$  and  $\bar{k}_{\text{perp}}$  —, although the data distribution does not suggest a preferential direction for greater permeability (Figure 8B), anisotropies evidencing a  $\bar{k}_{\text{perp}} > \bar{k}_{\text{para}}$  relationship tend to be more expressive than  $\bar{k}_{\text{para}} > \bar{k}_{\text{perp}}$  ones.

We analyzed the variation in rock permeability using mean values of the statistics from Table 2. Given the asymmetry, mean is the measure that better represents less frequent values resulting from variations within the same unit. Gravelly muddy sandstone (GMS) is the most permeable

unit and has the lowest permeability variance throughout its layers. MS presents the lowest permeability, followed by SGMS. Both have the highest variability as to permeability, in some cases reaching a value twice as high as that of GMS. The high coefficient of variation of the data reflects the heterogeneity of the lithological units, showing the high permeability variance that the same rocky unit can present.

Figure 9 presents the spatial distribution of permeability of each sampled point and highlights the influence of lithology and structures (faults and deformation bands). The defined permeability intervals were grounded in the basic statistics of the three directions to include the main quartiles, minimum, maximum, and mean data.

Due to the logarithmic distribution of permeability, the geostatistical stages were based on the logarithmic transformation of data. This transformation is also done to minimize the effects of extreme variations within data points and obtain a well-defined spatial distribution (Zhao et al., 2014). Considering the two-dimensional aspect of the data obtained in outcrop analogues and the sampling system



F1: fault 1.

**Figure 6.** Histograms of all permeability readings (data with outliers):  $\bar{M}$  (mean);  $Q_2$  (median);  $\sigma$  (standard deviation); IQR (interquartile range); min (minimum); max (maximum); CV (coefficient of variation in %). The first and last histogram intervals were visually changed in relation to the others only to highlight the main ranges of values. Basic statistics were calculated according to the data set and not the histogram ranges.

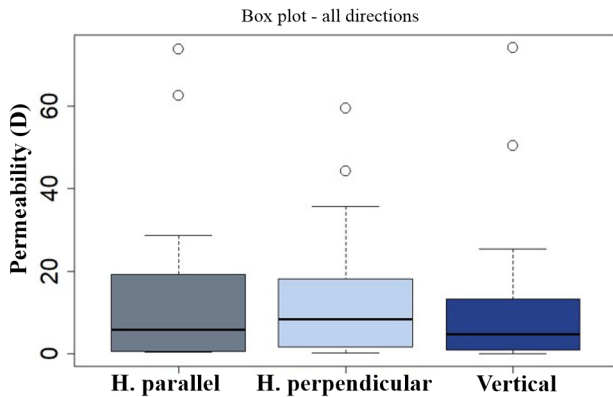
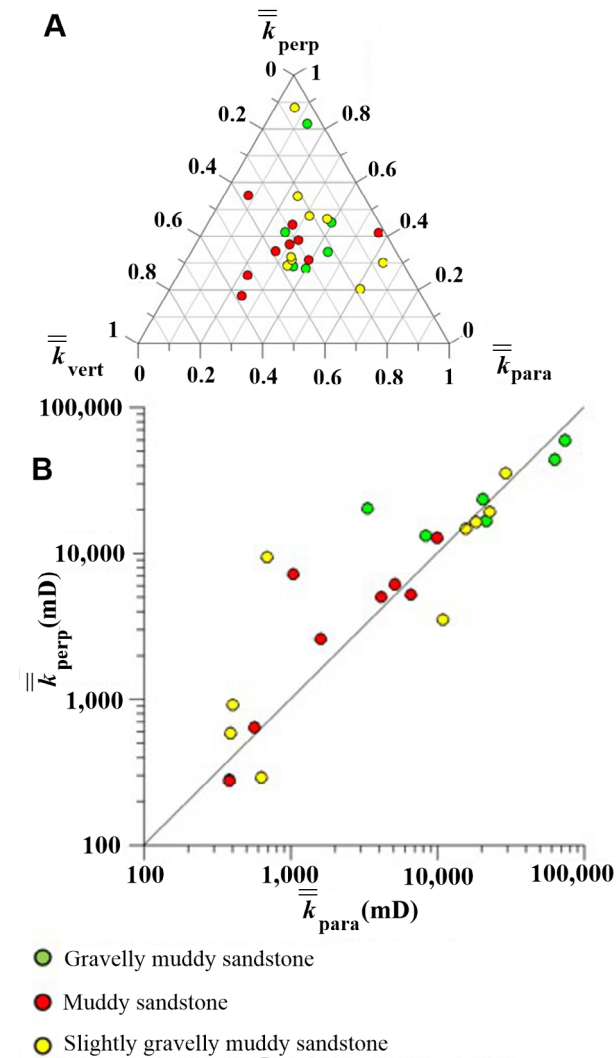


**Figure 7.** Box plot of median permeability values based on the directions.

concerning spatial correlation, the variographic analysis was developed for the horizontal flow perpendicular to the fault and the vertical flow, taking into account the 24 points tested according to the deterministic sampling. The accuracy of semivariance estimates is proportional to the number of samples, and omnidirectional semivariograms have more pairs than directional ones when all directions are considered in the calculation. Therefore, due to the limited amount of data, omnidirectional semivariograms were used to model spatial continuity to obtain the highest number of pairs and, consequently, improve the reliability of the analyzed semi-variogram. The term “omnidirectional” corresponds to the pair search angle in the semivariogram analysis; in this case, all directions are considered.





$\bar{k}_{\text{perp}}$ : characteristic permeability of horizontal flow perpendicular to the fault;  $\bar{k}_{\text{para}}$ : characteristic permeability of horizontal flow parallel to the fault;  $\bar{k}_{\text{vert}}$ : characteristic permeability of vertical flow.

**Figure 8.** (A) Ternary diagram showing the degree of anisotropy of the samples based on the dispersion in relation to the isotropic center. The permeability values were proportionally recalculated; (B) chart of the relationship between the characteristic permeability of horizontal flow perpendicular to the fault  $\bar{k}_{\text{perp}}$  and the characteristic permeability of horizontal flow parallel to the fault  $\bar{k}_{\text{para}}$ .

The best fitted model in both directions was the exponential one (Figures 10 and 11). In this model, the sill is reached asymptotically, expressing, besides the practical range, an increasing variance, but in smaller proportions, not being considered spatial interdependence.

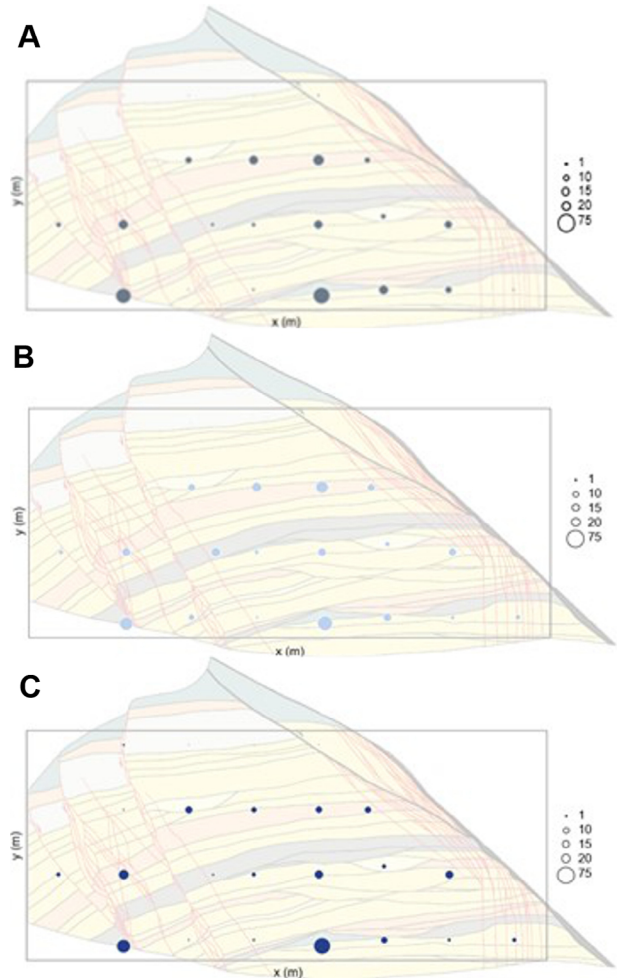


**Figure 9.** Bubble plot of the spatial distribution of permeability, in D, of the sampled points. (A)  $\bar{k}_{\text{para}}$  characteristic permeability of horizontal flow parallel to the fault; (B)  $\bar{k}_{\text{perp}}$  characteristic permeability of horizontal flow perpendicular to the fault; and (C) characteristic permeability of vertical flow  $\bar{k}_{\text{vert}}$ .

**Table 2.** Statistics of characteristic permeability values according to lithology.

	Characteristic permeability ( $\bar{k}$ )								
	Perpendicular			Parallel			Vertical		
	Median (D)	Mean (D)	CV (%)	Median (D)	Mean (D)	CV (%)	Median (D)	Mean (D)	CV (%)
GMS	21.86	29.55	61.83	20.89	31.61	35.08	10.38	25.72	50.61
MS	5.04	4.48	91.60	1.61	3.34	102.45	4.51	4.13	103.22
SGMS	9.48	11.28	104.45	10.72	10.85	100.80	3.28	8.62	113.42

CV: coefficient of variation; GMS: gravelly muddy sandstone; MS: muddy sandstone; SGMS: slightly gravelly muddy sandstone.

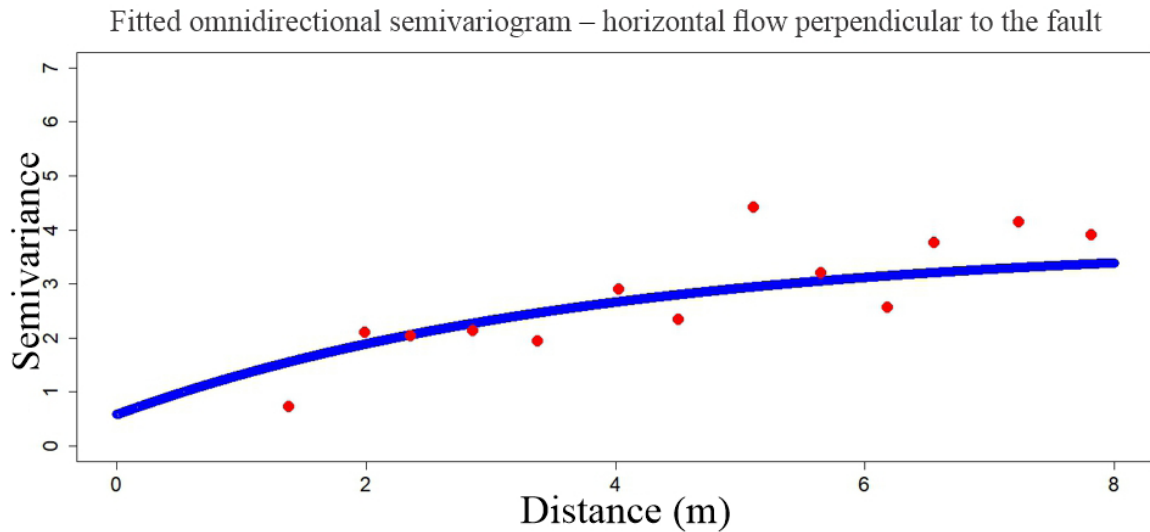


**Figure 10.** Fitted omnidirectional semivariogram of the logarithm of characteristic permeability of horizontal flow perpendicular to the fault  $\bar{k}_{\text{perp}}$ .

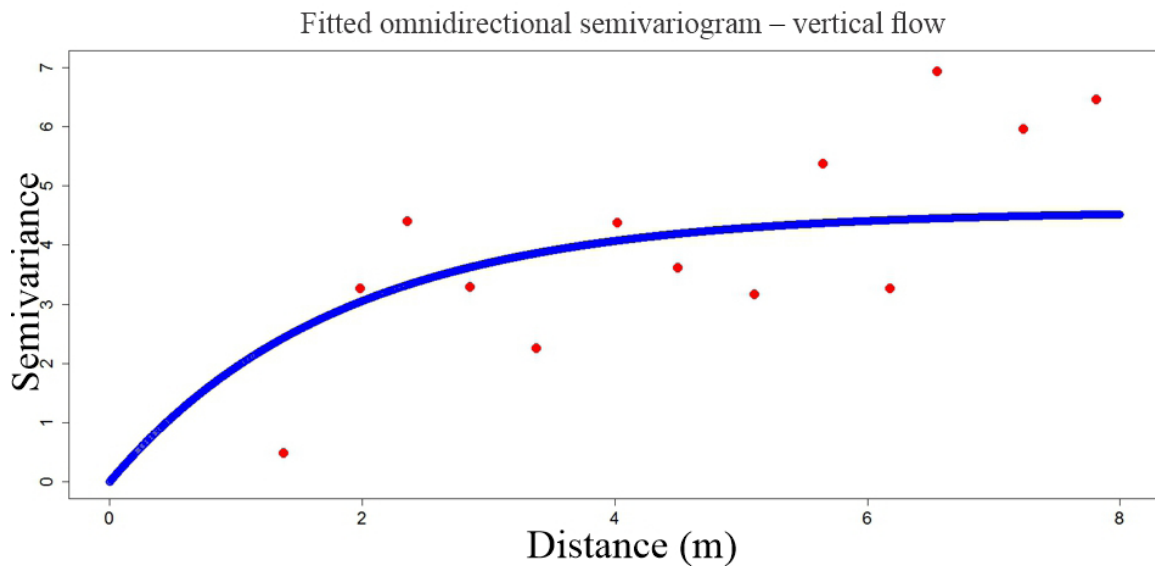


**Figure 11.** Fitted omnidirectional semivariogram of the logarithm of characteristic permeability of vertical flow  $\bar{k}_{\text{vert}}$ .

The adjustment led to a nugget effect of 0.58 and 0, a sill of 3.20 and 4.57, and a practical range of 3.80 and 1.81 m for  $\bar{k}_{\text{perp}}$  and  $\bar{k}_{\text{vert}}$ , respectively. As expected for geological media with superposition and interleaving layers (Pyrz and Deutsch, 2014; Ren et al., 2019), the range in the horizontal direction was greater than in the vertical one, as the first is parallel to the continuity of layers, while the second is perpendicular to them.

Based on semivariogram adjustments, ten simulations were generated for each direction — vertical and horizontal perpendicular to the fault. The simulation chosen was the one with the greatest similarity with the permeability distribution and structural and stratigraphic arrangement of the outcrop. Figure 12 presents the simulation chosen for  $\bar{k}_{\text{perp}}$  and its comparison with the outcrop section.

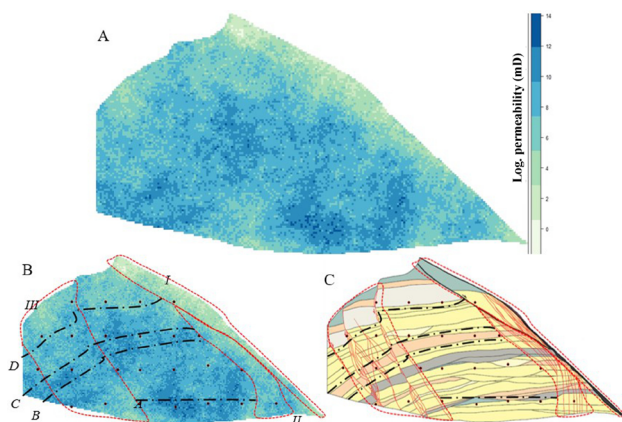


**Figure 12.** Simulation of the characteristic permeability of horizontal flow perpendicular to the fault  $\bar{k}_{\text{perp}}$ . (A) Simulation chosen for the criterion of better structural and stratigraphic representation of the outcrop; (B) spatial sample distribution in the simulation (black dots) and polygons that highlight some features well represented by the simulation when compared to (C) the outcrop section. The belts correspond to the natural permeability logarithm.

The control points, used to help simulate the region close to the fault, efficiently represented the reduced permeability attributed to this structure, as shown in the highlighted polygon I. Highlighted polygons II and III illustrate the influence of deformation bands on the reduction of permeability (Rotava, 2017; Vogel et al., 2019). Polygon II represents the band cluster that vertically extends from the base of the section and becomes parallel and adjacent to the main fault of the section. Polygon III has a less permeable belt (lighter color), elongated as per the band cluster in the southern part of the outcrop, which varies according to lithology, evidencing that the influence of the deformation band on permeability depends on the rock. As stated by Ballas et al. (2015), lithological characteristics may influence the permeability variance produced by cataclastic bands. Among them, high porosity and coarser and relatively well-selected grains can favor greater permeability contrasts in the presence of bands.

The difference in permeability according to lithology is another characteristic well represented by the simulation. In this regard, the low MS permeability (area above line D) and the high permeability in more gravelly sandstones, present at the base of the block (below line A) and in the conglomerate (between lines B and C), stand out. The slope of this last lithology was also represented in the southern portion of the block.

The  $\bar{k}_{\text{vert}}$  simulation, similar to that of  $\bar{k}_{\text{perp}}$ , was able to reproduce the permeability variance throughout the rocks and the proximity of structures (Figure 13). This similarity among the models generated is possibly related to the low

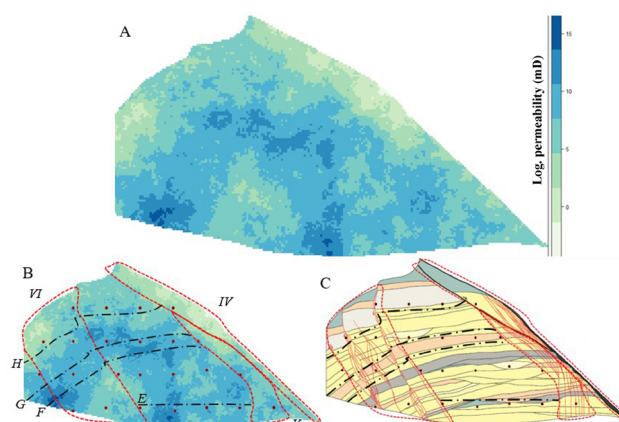


**Figure 13.** Simulation of the characteristic permeability of vertical flow  $\bar{k}_{\text{vert}}$ . (A) Simulation chosen for the criterion of better structural and stratigraphic representation of the outcrop; (B) spatial sample distribution in the simulation (black dots) and polygons that highlight some features well represented by the simulation when compared to (C) the outcrop section. The numbers used in the polygons follow those used in the simulation of the characteristic permeability of horizontal flow perpendicular to the fault  $\bar{k}_{\text{perp}}$ . The belts correspond to the natural permeability logarithm.

data anisotropy and the analysis according to omnidirectional semivariograms.

In both cases, most simulated data was consistent with the outcrop values. However, a small part extrapolated the range of values common to the outcrop due to the characteristics of simulation methods, which tend to generate minimal extrapolations.

Considering criteria 2 and 3, described in the “Method” section, when validating the model consistency in representing the spatial distribution of permeability in the outcrop, the simulations were statistically equivalent to the original samples in both directions (Figure 14). We emphasize that, in this step, the comparison with original data considers total deterministic sampling points and control points. The reason is that fault points were used as the base for the simulation, and basic statistics were used to describe the data set. The apparent better continuity between distribution intervals in the simulated histogram is associated with the larger sample size (15,038 data), while the original histograms have only 31 data and predominance of control points of lower permeability in their distribution (highlighted in red in Figure 14).

The semivariogram and its fitted model defined the behavior of the set of data pairs. Thus, this stage compared the simulated semivariogram to the semivariogram of experimental data (Figures 15 and 16) without considering the control points in the latter, as they were not used in the allocation of model parameters (range, sill, and nugget



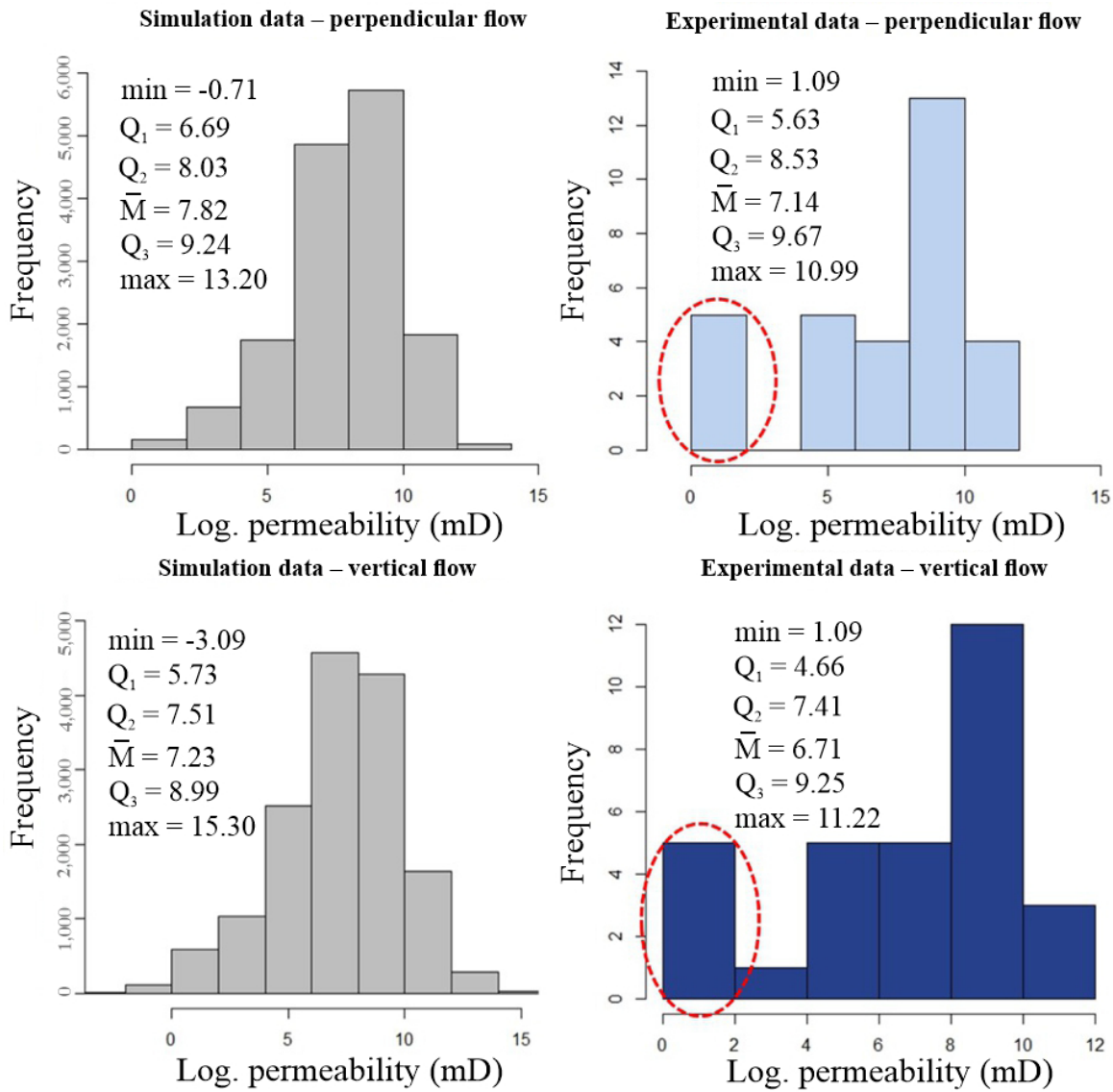


**Figure 14.** Histograms and basic statistics to compare simulation and experimental data (sampled points and control points). The red dashed line highlights control points with lower permeability in the distribution of data.

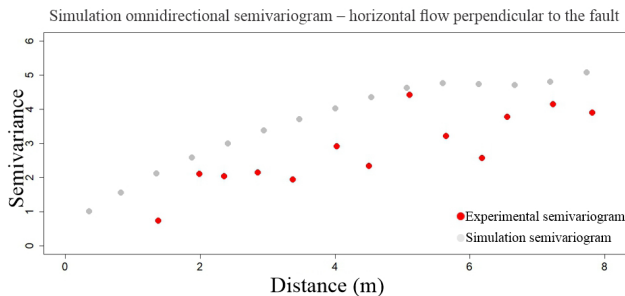


**Figure 15.** Comparison between omnidirectional semivariograms of experimental data and of simulated flow perpendicular to the fault.

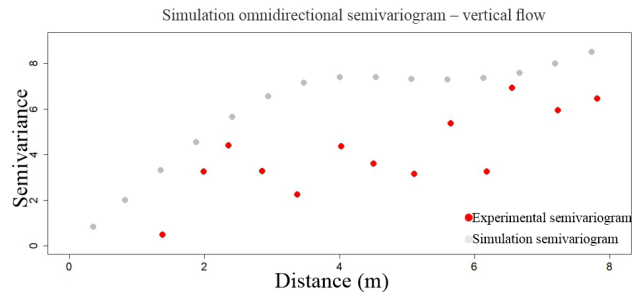


**Figure 16.** Comparison between omnidirectional semivariograms of experimental data and of simulated vertical flow.

effect). In both directions, the simulated semivariogram was similar to the experimental fitted model. Despite the differences in variance and range — more significantly in the vertical flow —, they were interpreted as acceptable since data were collected from only 24 points, and the simulated semivariogram considers control points and their weight in the interpolation, producing greater variance.

## CONCLUSION

Due to differences in the sedimentary characteristics of the Resende Formation and the influence of deformation bands and faults, the permeability readings of the 24 points, obtained from muddy and gravelly sandstones, resulted in high data variability. The  $\bar{k}$  of cells in the 3 directions ranged from  $10^{-5}$  to 74.2 D, expressing anisotropy considered commonly low and without preferential direction.

The variographic analysis and simulation did not include the horizontal flow parallel to the fault due to the bidimensionality related to the acquisition of outcrop analogue data and the sampling system regarding spatial correlation. For the analyzed directions, the best fitted model for the experimental semivariograms was the exponential model, with the horizontal range being greater than the vertical one. The use of control points in the faults proved to be efficient in the produced simulations. The result of the geostatistical model built with SGS was satisfactory, showing the impact of stratigraphy and structures — deformation band and fault — on fluid flow. With respect to consistency, the validation of the models was acceptable, taking into account the amount of experimental data and the greater variance imposed by control points.

In sum, the permeability models emphasized the importance of considering subseismic structures in the flow analysis of reservoirs since they can change the permeability of the material assessed.

## ACKNOWLEDGMENTS

We would like to thank PETROBRAS and the Agência Nacional do Petróleo, Gás Natural e Biocombustíveis (ANP) for the financial support, as part of the project “*Caracterização da deformação e de propriedades mecânicas e permoporosas de arenitos pouco consolidados*” (process 2014/00631-3, cooperation agreement 0050.0102131.16.9 UFRJ/COPPETEC/ANP/Petrobras); the Coordenação de Aperfeiçoamento de Pessoal de Nível Superior (CAPES) for the Master’s scholarship to the first author; and the Graduate Program in Geology of the Universidade Federal do Rio de Janeiro (UFRJ) for the opportunity to develop this research. We also thank our co-workers from the Laboratory of Experiments in Mechanics and Rock Technology at UFRJ (LEMETRO-UFRJ) for their

support in fieldwork and valuable discussions; Mr. José Luiz de Paiva Leijoto and Mr. Robson de Paiva Leijoto for allowing access to the study area; and the reviewers of this article for their relevant comments and suggestions.

## REFERENCES

- Associação Brasileira de Normas Técnicas (ABNT). (2016). *NBR 7181: Solo - Análise Granulométrica*. Rio de Janeiro: ABNT.
- Ballas, G., Fossen, H., Soliva, R. (2015). Factors controlling permeability of cataclastic deformation bands and faults in porous sandstone reservoirs. *Journal of Structural Geology*, 76, 1-21. <https://doi.org/10.1016/j.jsg.2015.03.013>
- Balsamo, F., Bezerra, F. H. R., Vieira M. M., Storti, F. (2013). Structural control on the Formation of iron-oxide concretions and liesegang bands in faulted, poorly lithified cenozoic sandstones of the Paraíba Basin, Brazil. *Geological Society of America Bulletin*, 125(5-6), 913-931. <https://doi.org/10.1130/B30686.1>
- Belila, A. M. P., Kuroda, M. C., Souza, J. P. P., Vidal, A. C., Trevisan, O. V. (2018). Petrophysical characterization of coquinas from Morro do Chaves Formation (Sergipe-Alagoas Basin) by x-ray computed tomography. *Geologia USP. Serie Científica*, 18(3), 3-13. <https://doi.org/10.11606/issn.2316-9095.v18-124101>
- Braga, L. P. V. (2014). *Introdução à geoestatística: Com programas em R*. Rio de Janeiro: E-papers.
- Brown, S., Smith, M. (2013). A transient-flow syringe air permeameter. *Geophysics*, 78(5), D307-D313. <https://doi.org/10.1190/GEO2012-0534.1>
- Camargo, J. E. N., Jensen, J. L. (2012). Analysis of fault permeability using mapping and flow modeling, Hickory sandstone aquifer, Central Texas. *Natural Resources Research*, 21(3), 395-409. <https://doi.org/10.1007/s11053-012-9181-5>
- Cao, R., Zee Ma, Y., Gomez, E. (2014). Geostatistical applications in petroleum reservoir modelling. *Journal of the Southern African Institute of Mining and Metallurgy*, 114, 625-629.
- Cressie, N. A. C. (1991). *Statistics for spatial data*. Michigan: J. Wiley.
- Farrell, N. J. C., Healy, D., Taylor, C. W. (2014). Anisotropy of permeability in faulted porous sandstones. *Journal of Structural Geology*, 63, 50-67. <https://doi.org/10.1016/j.jsg.2014.02.008>

- Fegh, A., Riahi, M. A., Norouzi, G. H. (2012). Permeability prediction and construction of 3d geological model: Application of neural networks and stochastic approaches in an Iranian gas reservoir. *Neural Computing and Applications*, 23(6), 1763-1770. <https://doi.org/10.1007/s00521-012-1142-8>
- Fiuza, B. O. (2019). *Análise multiescalar da deformação rúptil em rochas siliciclásticas pouco consolidadas (Formação Resende, Eoceno, Bacia de Volta Redonda, RJ)*. Dissertação (Mestrado). Rio de Janeiro: Instituto de Geociências - UFRJ.
- Fiuza, B. O., Mello, C. L., Ribeiro, C. S. (2020). Parâmetros de densidade de falhas e bandas de deformação em rochas siliciclásticas pouco consolidadas da Formação Resende, Eoceno, Bacia de Volta Redonda, estado do Rio de Janeiro. *Geologia USP. Série Científica*, 20(4), 39-52. <https://doi.org/10.11606/issn.2316-9095.v20-165065>
- Folk, R. L. (1974). *Petrology of Sedimentary Rocks*. Estados Unidos: Hemphill Publishing Co.
- Galvão, M. S., Barroso, E. V., Leão, M. F., Mello, C. L., Souza, J. A. B. (2018). Fault zones control on permeability of poorly lithified sandstone. In: 52nd US Rock Mechanics/ Geomechanics Symposium. Washington, D.C.: American Rock Mechanics Association.
- Hosseini, E., Gholami, R., Hajivand, F. (2019). Geostatistical modeling and spatial distribution analysis of porosity and permeability in the Shurijeh-B reservoir of Khangiran gas field in Iran. *Journal of Petroleum Exploration and Production Technology*, 9(2), 1051-1073. <https://doi.org/10.1007/s13202-018-0587-4>
- Leuangthong, O., McLennan, J. A., Deutsch, C. V. (2004). Minimum acceptance criteria for geostatistical realizations. *Natural Resources Research*, 13(3), 131-141. <https://doi.org/10.1023/B:NARR.0000046916.91703.bb>
- Maciel, I. B., Mello, C. L., Silva, A. T. (2017). Caracterização da deformação rúptil em afloramento da formação Resende, bacia de Volta Redonda, Estado do Rio de Janeiro. *Geologia USP. Série Científica*, 17(3), 113-124. <https://doi.org/10.11606/issn.2316-9095.v17-391>
- Negrão, A. P., Ramos, R. R. C., Mello, C. L., Sanson, M. S. R. (2015). Mapa geológico do cenozoico da região da bacia de Volta Redonda (RJ, segmento central do Rift Continental do Sudeste do Brasil): Identificação de novos grabens e ocorrências descontínuas, e caracterização de estágios tectonossedimentares. *Brazilian Journal of Geology*, 45(2), 273-291. <https://doi.org/10.1590/23174889201500020007>
- Pebesma, E. J., Wesseling, C. G. (1998). Gstat: a program for geostatistical modelling, prediction and simulation. *Computers & Geosciences*, 24(1), 17-31. [https://doi.org/10.1016/S0098-3004\(97\)00082-4](https://doi.org/10.1016/S0098-3004(97)00082-4)
- Pyrcz, M. J., Deutsch, C. V. (2014). *Geostatistical reservoir modeling*. 2. ed. Estados Unidos: Oxford University Press.
- R Core Team (2018). *R: A language and environment for statistical computing*. R Foundation for Statistical Computing, Vienna, Austria. Available at: <http://www.R-project.org>. Accessed on: Apr. 29, 2021.
- Ren, S., Yao, G., Zhang, Y. (2019). High-resolution geostatistical modeling of an intensively drilled heavy oil reservoir, the BQ 10 block, Biyang Sag, Nanxiang Basin, China. *Marine and Petroleum Geology*, 104, 404-422. <https://doi.org/10.1016/j.marpetgeo.2019.03.026>
- Riccomini, C., Sant'Anna, L. G., Ferrari, A. L. (2004). Evolução geológica do Rift Continental do Sudeste do Brasil. In: V. Mantesso-Neto, A. Bartorelli, C. Dal Ré Carneiro, B. B. Brito Neves (Eds.), *Geologia do Continente Sul-Americano: Evolução da Obra de Fernando Flávio Marques de Almeida* (p. 383-405). São Paulo: Beca.
- Rotava, T. (2017). *Caracterização macroscópica e microscópica de bandas de deformação em arenitos da Formação Resende (Eoceno, Rift Continental do Sudeste do Brasil)*. Trabalho de Conclusão de Curso (Bacharelado em Geologia). Rio de Janeiro: Instituto de Geociências - UFRJ.
- Sanson, M. S. R., Ramos, R. R. C., Mello, C. L. (2006). Bacias Sedimentares Brasileiras – Bacia de Volta Redonda. *Phoenix*, 88, 1-6.
- Slatt, R. M. (2006). *Stratigraphic Reservoir Characterization for Petroleum Geologist, Geophysicists and Engineers*. Amsterdã: Elsevier.
- Souza, A. M. (2013). *Proposta metodológica para o imageamento, caracterização, parametrização e geração de modelos virtuais de afloramentos*. Tese (Doutorado). Rio Grande do Norte: Instituto de Geociências - UFRN.
- Vogel, S. N., Mello, C. L., Silva, A. T. (2019). Aspectos tomográficos e microtomográficos de feições de deformação rúptil em arenitos pouco consolidados da Formação Resende (Bacia de Volta Redonda-RJ). *Anuário do Instituto de Geociências*, 42(1), 759-768. [https://doi.org/10.11137/2019\\_1\\_759\\_768](https://doi.org/10.11137/2019_1_759_768)



Wentworth, C. K. (1922). A scale of grade and class terms for clastic sediments. *Journal of Sedimentary Petrology*, 30, 377-392. <https://doi.org/10.1086/622910>

Wilson, C. E., Aydin, A., Durlifsky, L. J., Boucher, A., Brownlow, D. T. (2011). Use of outcrop observations, geostatistical analysis, and flow simulation to investigate structural controls on secondary hydrocarbon migration in

the Anacacho Limestone, Uvalde, Texas. *AAPG Bulletin*, 95(7), 1181-1206. <https://doi.org/10.1306/11191010069>

Zhao, S., Zhou, Y., Wang, M., Xin, X., Chen, F. (2014). Thickness, porosity, and permeability prediction: comparative studies and application of the geostatistical modeling in an Oil field. *Environmental Systems Research*, 3, 1-24. <https://doi.org/10.1186/2193-2697-3-7>